A Numerical Investigation of Metamaterial Antireflection Coatings

Hou-Tong Chen *, Jiangfeng Zhou, John F. O'Hara, and Antoinette J. Taylor
MPA-CINT, MS K771, Los Alamos National Laboratory, Los Alamos, NM 87545, USA
* Email: chenht@lanl.gov

Abstract: Electromagnetic metamaterials have emerged as a new class of effective media where exotic properties are determined from structural geometry and dimensions of the basic building blocks, or meta-atoms. Through such a bottom-up approach, metamaterials have found applications in the construction of terahertz functional devices and components with unprecedented performance. In this paper, we numerically investigate planar metamaterials that function as antireflection coatings for dielectric surfaces, suppressing the reflection and enhancing the transmission. We show in detail how the metamaterial structures and losses affect the antireflection performance. We also show the angular dependence of metamaterial antireflection for both transverse electric and transverse magnetic polarizations, which reveals a tunable Brewster's angle behavior.

Keywords: metamaterials, antireflection coatings, Terahertz, simulations

doi: 10.11906/TST.066-073.2010.06.06

1. Introduction

Light reflection at a dielectric surface is undesirable in many situations, for example, causing insertion losses in photonic devices and optical components. This is a particularly severe issue in the far infrared or terahertz (THz) frequency range due to the generally low power available in many THz systems, and the fact that many THz devices and components are fabricated on substrates with high dielectric constant. Therefore, THz antireflection coatings are highly desirable to suppress the reflection and enhance the transmission. Antireflection coatings comprised of single or multiple layered dielectric thin films via vacuum depositions have long been the solution in the optical regime, however, this approach is quite technically challenging in the longer wavelength THz frequency range. The simplest antireflection approach, the quarter-wave antireflection coating, requires a refractive index matching, $n_2 = \sqrt{n_1 n_3}$, and a coating thickness, $d = \lambda/4$, where n_2 is the refractive index of the coating material, n_1 and n_3 are the refractive indices of two bounding dielectric media, and λ is the wavelength in the coating material [1]. It is therefore limited by the availability of natural materials, i.e., it might be difficult to find appropriate coating materials that satisfy the index-matching requirement and are also suitable for thick film coating ranging from tens to hundreds microns. The latter is necessary due to the long wavelength of THz radiation.

There have been a few efforts developing antireflection coatings at THz frequencies, though they are specific to certain substrates and/or coating materials. The first approach follows the conventional interference principle and creates the antireflection coating by various means: gluing thin wafers [2,3], vacuum deposition of silica [4], coating with polymers such as polyethylene [5], parylene [6], and polyimide [7], and plasma-enhanced chemical-vapor deposition of single layered silicon oxide [8] or multiple layered amorphous silicon and silicon oxide [9]. As pointed out, the antireflection coatings require an index matching of the coating materials, and they have to be quite thick, at least several tens of microns. The second antireflection approach is through fabricating artificial dielectric structures, or surface relief

structures, to achieve impedance matching with a gradient index [10-12], or to create an effective index value satisfying quarter-wave antireflection [13]. This approach, however, demands special high precision fabrication procedures, in addition to the fact that substrate surfaces are no longer flat or smooth, limiting their application to many photonic devices. The last approach is to coat substrate surfaces with thin metal films having very precisely controlled thickness [14-16]. It has the advantage of broadband performance, but suffers from high loss and therefore prevents any enhancement in the transmission.

Metamaterials with designed and controllable electromagnetic properties have enabled THz device applications with unprecedented performance, for instance, THz switches and modulators [17-23] using semiconductors as integrated parts of the metamaterial elements. It has also been demonstrated that metamaterials can match the free space impedance and result in perfect absorption of THz radiation [24,25]. A recent review of metamaterials in the THz regime can be found in Ref. [26]. Recently we have proposed and demonstrated that metamaterials can be used to achieve excellent antireflection performance and transmission enhancement over a wide range of incidence angle within a reasonably narrow bandwidth [27]. Its mechanism was elucidated when considering the metamaterial coatings as a thin slab, where the interfaces tune the reflection magnitude and impart large phase shifts satisfying the antireflection requirements [27]. The destructive and constructive interferences result in the suppression of reflectance and the enhancement of transmittance. This approach differs significantly from impedance matching to free space using metamaterials [28,29], i.e., we are using metamaterials to match impedances between two dielectric media. In this paper we provide a further numerical investigation of metamaterial antireflection, focusing on how the antireflection performance is affected by the spacer dielectric constant and thickness, as well as the dielectric and metal losses. We also show the angular dependent antireflection for transverse magnetic (TM) and transverse electric (TE) polarizations, which reveal a tunable “Brewster’s angle” for both polarizations.

2. Metamaterial antireflection design and numerical simulation methods

The metamaterial antireflection coating consists of a square array of metallic electric split-ring resonators (SRRs) [30] and a metallic mesh [31], which are separated by a dielectric spacer layer, on a substrate surface. The unit cell is schematically shown in Fig. 1, where we assume lossless

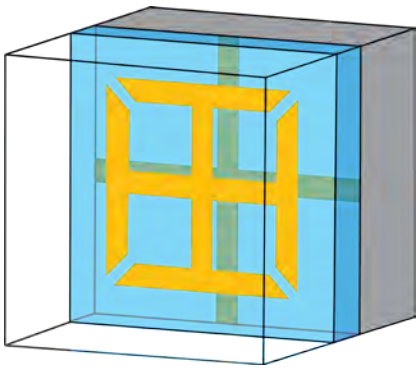

Fig. 1 Schematic of the metamaterial antireflection coating on a dielectric surface. The metamaterial coating consists of a mesh and an electric split-ring resonator array separated by a dielectric spacer layer.

substrates with a dielectric constant of ε_s = 12.0, a value that is typical for many THz substrates. The SRRs have outer dimensions of 36 μm, a gap width of 4 μm, and a periodicity of 46 μm, and the width of metal lines is 4 μm. Finite-element numerical simulations in the frequency domain are carried out using the commercial available package CST Studio Suite [32]. A periodic boundary condition and hexahedral mesh are applied when metal and dielectric losses are neglected; otherwise perfect electric conducting and perfect magnetic conducting boundaries and tetrahedral mesh are used. A pair of waveguide ports is applied on the front surface of vacuum space and on the back surface of the substrate. The simulations result in complex S-parameters, from which we obtain the frequency dependent reflectance $R = |S_{11}|^2$ and transmittance $T = |S_{21}|^2$. Under normal incidence, we vary the spacer dielectric constant and thickness, as well as the dielectric and metal losses, to observe their effects on the reflection suppression and transmission enhancement. We also vary the incident angle to observe the reflectance for both TM and TE polarizations with different spacer thicknesses, where no loss has been assumed.

3. Dependence on the spacer dielectric and metal properties

First we investigate the THz reflection and transmission under normal incidence. A periodic boundary condition is applied assuming lossless metal and dielectric spacer. The spacer dielectric constant can be arbitrary assumed, and here we take two extreme values, ε_s = 2.0, which is quite small, and ε_s = 14.0, which is larger than that of the substrate. It should be noted that the spacer materials with these dielectric constants couldn't be used for the quarter-wave antireflection purpose. The reflectance and transmittance as a function of spacer thickness are shown in Fig. 2.

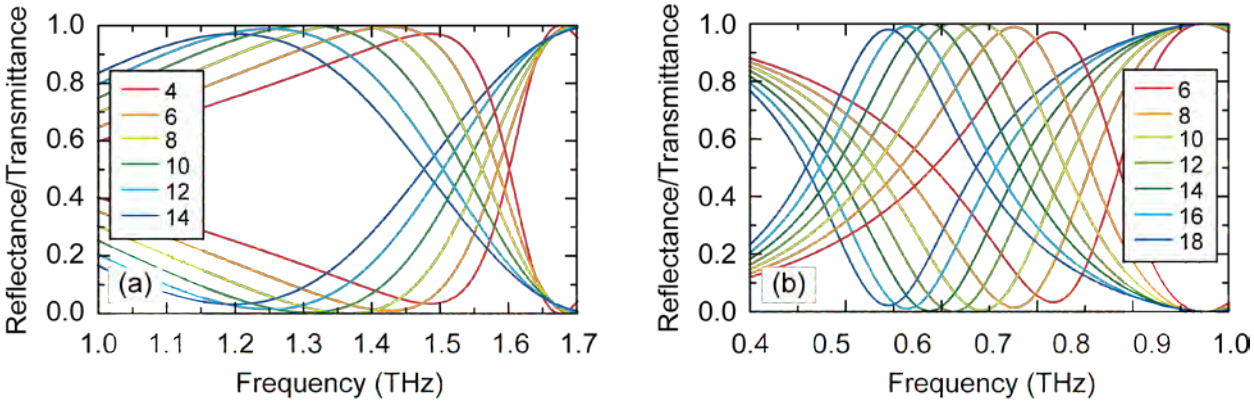

Fig. 2 Reflectance and transmittance spectra as a function of spacer thickness at the metamaterial-coated substrate surface under normal incidence, with the spacer dielectric constant (a) ε_s = 2.0 and (b) ε_s = 14.0. The legend units are microns.

For all the spacer thicknesses simulated here, there are reduced reflectance and enhanced transmittance over a frequency band as compared to a bare substrate surface. When the spacer thickness is small, there still remains a certain amount of reflection, and it continuously decreases and shifts to lower frequencies as the spacer thickness increases. The simulations show that for any spacer dielectric constant, there is always an optimized spacer thickness, which is 8 μm for ε_s = 2.0 and 12 μm for ε_s = 14.0, with which reflectance of 0% and transmittance of 100% can be

achieved. Further increasing the spacer thickness, however, will degrade the antireflection performance. These metamaterial coatings are much thinner than those in quarter-wave antireflection coatings operating at the same frequencies, and also require no index matching. The results in Fig. 2 reveal that the antireflection performance is less sensitive to the spacer thickness when the spacer dielectric constant is smaller, and also has a broader bandwidth.

Losses have to be included in real metamaterial antireflection coatings, and arise from the finite conductivity of metal and the dielectric loss in the spacer layer. In Fig. 3 we show the thickness dependent reflectance and transmittance which are compared between two cases: i) considering metal as perfect electrical conductor (PEC) and using lossless spacer with $\varepsilon_s = 4.0$; and ii) using lossy gold with default conductivity (4.5×10^7 *S/m*) and the spacer with $\varepsilon_s = 4.0$ and loss tangent of 0.02. The latter closely simulates the real metamaterial coatings using low loss polymers such as polyimide [25,33] as the dielectric spacer. When there is no loss from the metal and dielectric spacer, perfect antireflection is achieved at about 1.0 *THz* with the spacer thickness of 10 μm, i.e., 0% reflectance and 100% transmittance. After considering both the metal and dielectric losses, zero reflectance is still observed at 0.95 *THz* with the spacer thickness of 12 μm (the reflectance at 1.0 *THz* with 10 μm spacer thickness remains small), and 89% transmittance is achieved as compared to an expected transmittance value of 70% for the bare substrate surface, which is consistent with our experimental observations [27]. These results reveal that near zero reflectance can always be achieved. The losses mainly cause the reduction in transmittance, which is still fairly high due to the advantageous off-resonance operation of the metamaterial antireflection.

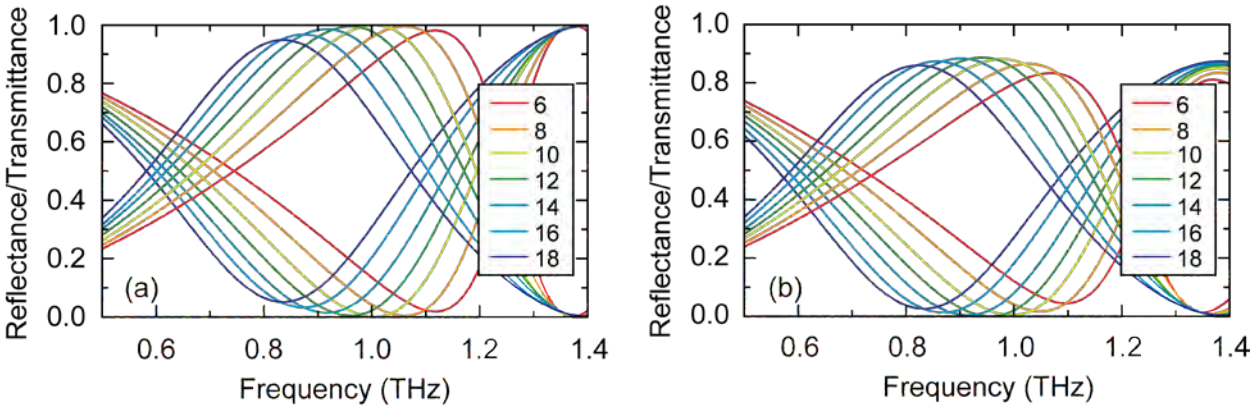

Fig. 3 Reflectance and transmittance spectra as a function of spacer thickness of the metamaterial-coated substrate surface under normal incidence. (a) Considering the metal as a perfect electric conductor and using a lossless spacer dielectrics with $\varepsilon_s = 4.0$. (b) Using lossy gold with the default conductivity in CST, and assuming the lossy spacer dielectrics $\varepsilon_s = 4.0$ and a loss tangent of 0.02. The legend units are microns.

4. Angular and polarization dependence

Previously we have experimentally observed that the metamaterial antireflection coatings are able to operate over a wide range of incident angles, and they behave a little differently for TM and TE polarizations [27]. Here we simulate the angular dependence of reflectance for TM and TE polarizations, either at or deviating from the optimized spacer thickness. For simplicity, losses

are not included, and the spacer dielectric constant is ε_s = 4.0. Fig. 4(a) and 4(b) show the reflectance for TM and TE polarizations, respectively, at the optimized spacer thickness of 10 μm. At frequencies away from the operation frequency of 1 *THz*, we clearly observe a significantly different angular dependence. At the antireflection frequency of about 1 *THz*, however, they show the almost identical dependence on the incident angles, which are shown in Fig. 4(c) and 4(d). Under normal incidence, the reflectance is nearly zero. Increasing the incident angle will

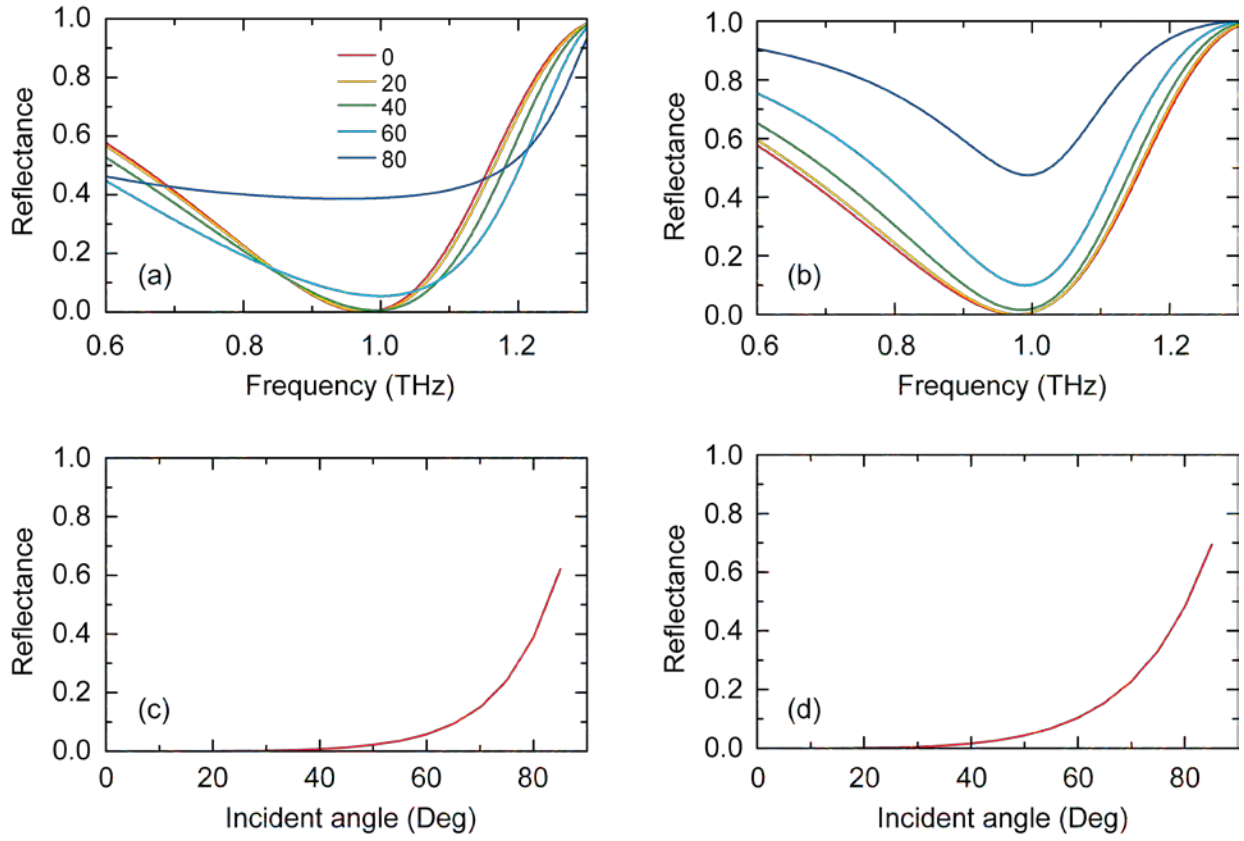

Fig. 4 Reflectance dependence on the incident angle, (a) and (c) for TM polarization, and (b) and (d) for TE polarization, with the optimized spacer thickness of 10 μm.

slowly increase the reflectance monotonically with R < 1% up to 35°. Further increasing the incident angle the reflectance will continue to increase but it is still less than 10% at incident angles up to 60°. The polarization insensitive property in metamaterial antireflection coatings is obviously advantageous over the conventional approaches such as quarter-wave antireflection.

Deviating from the optimized spacer thickness, even at the designed antireflection frequency, the TM and TE reflectance behaves differently. Fig. 5 shows the simulated angular dependence of the reflectance at the antireflection frequencies, with the spacer thickness of 6 μm and 16 μm, which are thinner and thicker, respectively, than the optimized spacer thickness of 10 μm. The antireflection frequency shifts as shown in Fig. 3, and the reflectance under normal incidence is still low, only 2~3%. In the case that the spacer thickness is less than the optimized value, TE reflectance increases monotonically with the incident angle, as shown in Fig. 5(a), while TM reflectance decreases first and than increases, with zero reflectance near 45°, which is similar to the Brewster's angle. When the spacer thickness is larger than the optimized value, the angular

dependence is reversed for TM and TE polarizations, as shown in Fig. 5(b). Now the TM reflectance increases monotonically with the incident angle, while the TE reflectance decreases first then increases, showing a Brewster's angle-like behavior. For a dielectric surface, this Brewster's angle-like behavior for TE polarization is not possible unless utilizing materials where the magnetic permeability is not equal to unity.

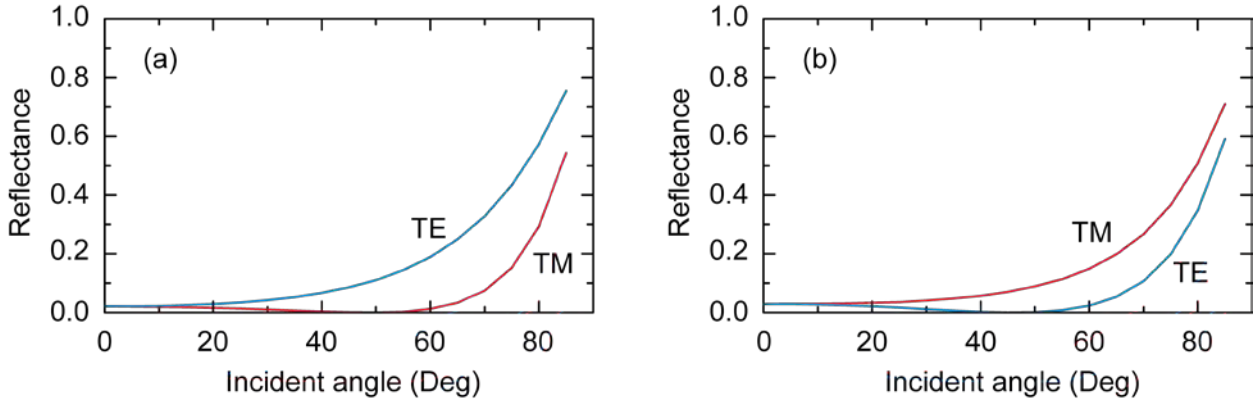

Fig. 5 Angular dependence of reflectance for TM and TE polarizations. (a) Spacer thickness is 6 μm, which is thinner than the optimized thickness, and (b) spacer thickness is 16 μm, which is thicker than the optimized spacer thickness.

5. Conclusions

We have numerically investigated a novel antireflection approach using metamaterials. The results are consistent with earlier experimental observations. The metamaterial antireflection coatings do not require materials having a matched refractive index, and they can also be much thinner than conventional antireflection (quarter-wave) coatings. The metal and dielectric losses have little effect on the reflectance. They reduce the transmittance, but ~90% transmittance should be still achievable. The metamaterial antireflection is polarization independent when the spacer thickness is optimized. As the spacer thickness deviates from the optimized value, the TM and TE reflections behave differently. Particularly, when the spacer thickness is larger, TE reflectance reveals a Brewster's angle-like behavior, which cannot be observed for non-magnetic dielectric surfaces. The metamaterial antireflection will significantly suppress the insertion losses in many THz photonic devices and components, and it can be integrated to achieve many novel metamaterial functionalities.

We acknowledge support from the Los Alamos National Laboratory LDRD Program. This work was performed, in part, at the Center for Integrated Nanotechnologies, a US Department of Energy, Office of Basic Energy Sciences Nanoscale Science Research Center operated jointly by Los Alamos and Sandia National Laboratories. Los Alamos National Laboratory, an affirmative action/equal opportunity employer, is operated by Los Alamos National Security, LLC, for the National Nuclear Security Administration of the US Department of Energy under contract DE-AC52-06NA25396.

References

[1] M. Born and E. Wolf, *Principles of optics*, Pergamon Press, New York, 6th ed, (1980).

[2] K. Kawase and N. Hiromoto, Terahertz-wave antireflection coating on Ge and GaAs with fused quartz, *Appl. Opt.* 37, 1862-1866, (1998).

[3] K. Kawase, N. Hiromoto, and M. Fujiwara, Terahertz-wave antireflection coating on Ge wafer using optical lapping method, *Electron. Commun. Jpn. 2* 83, 10-15, (2000).

[4] D. B. Fenner, J. M. Hensley, M. G. Allen, J. Xu, and A. Tredicucci, Antireflection coating for external-cavity quantum cascade laser near 5 THz, *Mater. Res. Soc. Symp. Proc.* 1016, 1016-CC07-03, (2007).

[5] C. R. Englert, M. Birk, and H. Maurer, Antireflection coated, wedged, single-crystal silicon aircraft window for the far-infrared, *IEEE Trans. Geosci. Remote Sens.* 37, 1997-2003, (1999).

[6] A. J. Gatesman, J. Waldman, M. Ji, C. Musante, and S. Yngvesson, An anti-reflection coating for silicon optics at terahertz frequencies, *IEEE Microwave Guided Wave Lett*. 10, 264-266, (2000).

[7] J. Lau, J. Fowler, T. Marriage, L. Page, J. Leong, E. Wishnow, R. Henry, E. Wollack, M. Halpern, D. Marsden, and G. Marsden, Millimeter-wave antireflection coating for cryogenic silicon lenses, *Appl. Opt.* 45, 3746-3751, (2006).

[8] I. Hosako, Antireflection coating formed by plasma-enhanced chemical-vapor deposition for terahertz-frequency germanium optics, *Appl. Opt.* 42, 4045-4048, (2003).

[9] I. Hosako, Multilayer optical thin films for use at terahertz frequencies: method of fabrication, *Appl. Opt*. 44, 3769-3773, (2005).

[10] Y.-F. Huang, S. Chattopadhyay, Y.-J. Jen, C.-Y. Peng, T.-A. Liu, Y.-K. Hsu, C.-L. Pan, H.-C. Lo, C.-H. Hsu, Y.-H. Chang, C.-S. Lee, K.-H. Chen, and L.-C. Chen, Improved broadband and quasiomnidirectional anti-reflection properties with biomimetic silicon nanostructures, *Nature Technol.* 2, 770-774, (2007).

[11] Y. W. Chen, P. Y. Han, and X.-C. Zhang, Tunable broadband antireflection structures for silicon at terahertz frequency, *Appl. Phys. Lett.* 94, 041106, (2009).

[12] C. Brückner, B. Pradarutti, O. Stenzel, R. Steinkopf, S. Riehemann, G. Notni, and A. Tünnermann, Broadband antireflective surface-relief structure for THz optics, *Opt. Express* 15, 779-789, (2007).

[13] A. Wagner-Gentner, U. U. Graf, D. Rabanus, and K. Jacobs, Low loss THz window, *Infrared Phys. Technol.* 48, 249-253, (2006).

[14] J. Kröll, J. Darmo, and K. Unterrainer, High-performance terahertz electro-optic detector, *Electro. Lett.* 40, 763-764, (2004).

[15] J. Kröll, J. Darmo, and K. Unterrainer, Metallic wave-impedance matching layers for broadband terahertz optical systems, *Opt. Express* 15, 6552-6560, (2007).

[16] A. Thoman, A. Kern, H. Helm, and M. Walther, Nanostructured gold films as broadband terahertz antireflection coatings, *Phys. Rev. B* 77, 195405, (2008).

[17] H.-T. Chen, W. J. Padilla, J. M. O. Zide, A. C. Gossard, A. J. Taylor, and R. D. Averitt, Active terahertz metamaterial devices, *Nature* 444, 597-600, (2006).

[18] H.-T. Chen, W. J. Padilla, M. J. Cich, A. K. Azad, R. D. Averitt, and A. J. Taylor, A metamaterial solid-state terahertz phase modulator, *Nature Photon.* 3, 148-151, (2009).

[19] H.-T. Chen, H. Lu, A. K. Azad, R. D. Averitt, A. C. Gossard, S. A. Trugman, J. F. O'Hara, and A. J. Taylor,

Electronic control of extraordinary terahertz transmission through subwavelength metal hole arrays, *Opt. Express* 16, 7641-7648, (2008).

[20] W. J. Chan, H.-T. Chen, A. J. Taylor, I. Brener, M. J. Cich, and D. M. Mittleman, A spatial light modulator for terahertz beams, *Appl. Phys. Lett.* 94, 213511, (2009).

[21] W. J. Padilla, A. J. Taylor, C. Highstrete, M. Lee, and R. D. Averitt, Dynamical electric and magnetic metamaterial response at terahertz frequencies, *Phys. Rev. Lett*. 96, 107401, (2006).

[22] H.-T. Chen, W. J. Padilla, J. M. O. Zide, S. R. Bank, A. C. Gossard, A. J. Taylor, and R. D. Averitt, Ultrafast optical switching of terahertz metamaterials fabricated on ErAs/GaAs nanoisland superlattices, *Opt. Lett.* 32, 1620-1622, (2007).

[23] H.-T. Chen, J. F. O'Hara, A. K. Azad, A. J. Taylor, R. D. Averitt, D. B. Shrekenhamer and W. J. Padilla, Experimental demonstration of frequency-agile terahertz metamaterials, Nature Photon. 2, 295-298, (2008).

[24] N. I. Landy, S. Sajuyigbe, J. J. Mock, D. R. Smith, and W. J. Padilla, Perfect metamaterial absorber, *Phys. Rev. Lett.* 100, 207402, (2008).

[25] H. Tao, N. I. Landy, C. M. Bingham, X. Zhang, R. D. Averitt, and W. J. Padilla, A metamaterial absorber for the terahertz regime: Design, fabrication and characterization, *Opt. Express* 16, 7181-7188, (2008).

[26] W. Withayachumnankul and D. Abbott, Metamaterials in the terahertz regime, *IEEE Photonics J.* 1, 99-118, (2009)

[27] H.-T. Chen, J. Zhou, J. F. O'Hara, F. Chen, A. K. Azad, and A. J. Taylor, Antireflection coating using planar metamaterials, arXiv:1002.2305v1, (2010).

[28] J. W. Lee, M. A. Seo, J. Y. Sohn, Y. H. Ahn, D. S. Kim, S. C. Jeoung, Ch. Lienau, andQ-Han Park, Invisible plasmonic meta-materials through impedance matching to vacuum, *Opt. Express* 13, 10681-10687, (2005).

[29] J. B. Pendry, D. Schurig, and D. R. Smith, Controlling electromagnetic fields, *Science* 312, 1780-1782, (2006).

[30] H.-T. Chen, J. F. O'Hara, A. J. Taylor, R. D. Averitt, C. Highstrete, M. Lee, and W. J. Padilla, Complementary planar terahertz metamaterials, *Opt. Express* 15, 1084-1095, (2007).

[31] R. Ulrich, Far-infrared properties of metallic mesh and its complementary structure, *Infrared Phys.* 7, 37-55, (1967).

[32] CST Studio Suite, http://www.cst.com/, (2009).

[33] A. K. Azad, H.-T. Chen, X. Lu, J. Gu, N. R. Weisse-Bernstein, E. Akhadov, A. J. Taylor, W. Zhang, and J. F. O'Hara, Flexible quasi-three-dimensional terahertz electric metamaterials, *Terahertz Science and Technology* 2, 15-22, (2009).